Journal of Biomedical Optics

SPIEDigitalLibrary.org/jbo

Application of laser pulse stretching scheme for efficiently delivering laser energy in photoacoustic imaging

Tianheng Wang
Patrick D. Kumavor
Quing Zhu

SPIE

Application of laser pulse stretching scheme for efficiently delivering laser energy in photoacoustic imaging

Tianheng Wang, Patrick D. Kumavor, and Quing Zhu
University of Connecticut, Electrical and Computer Engineering Department, Storrs, Connecticut 06269

Abstract. High-energy and short-duration laser pulses are desirable to improve the photoacoustic image quality when imaging deeply seated lesions. In many clinical applications, the high-energy pulses are coupled to tissue using optical fibers. These pulses can damage fibers if the damage threshold is exceeded. While keeping the total energy under the Food and Drug Administration limit for avoiding tissue damage, it is necessary to reduce the peak intensity and increase the pulse duration for minimizing fiber damage and delivering sufficient light for imaging. We use laser-pulse-stretching to address this problem. An initial 17-ns pulse was stretched to 27 and 37 ns by a ring-cavity laser-pulse-stretching system. The peak power of the 37-ns stretched pulse reduced to 42% of the original, while the fiber damage threshold was increased by 1.5-fold. Three ultrasound transducers centered at 1.3-, 3.5-, and 6-MHz frequencies were simulated, and the results showed that the photoacoustic signal of a 0.5-mm-diameter target obtained with 37-ns pulse was about 98, 91, and 80%, respectively, using the same energy as the 17-ns pulse. Simulations were validated using a broadband hydrophone. Quantitative comparisons of photoacoustic images obtained with three corresponding transducers showed that the image quality was not affected by stretching the pulse. [DOI: 10.1117/1.JBO.17.6.061218]

Keywords: laser pulse stretching; photoacoustic imaging; fiber damage.

Paper 11533SS received Sep. 20, 2011; revised manuscript received Feb. 24, 2012; accepted for publication Feb. 27, 2012; published online May 10, 2012.

1 Introduction

Photoacoustic imaging has emerged as a promising biomedical imaging technique and demonstrated great potential for medical applications,[1,2] including imaging skin tissue,[3] brain vasculature,[4–6] cancerous lesions in the breast,[7] and ovarian tissue.[8,9] Near-infrared short-pulsed laser light is employed for tissue irradiation, and an ultrasound transducer is used to receive the photoacoustic signals generated by the tissue from absorption of the light. In many clinical applications, including intravascular,[10,11] endoscopic,[12] and transvaginal applications, optical fibers are widely used to deliver the laser beam to the imaged tissue. During the photoacoustic imaging of deeply seated lesions lying several centimeters below the tissue surface, high-energy and short duration laser pulses are often employed to improve the image quality. These high peak intensity pulses can, however, damage an optical fiber input face during light coupling if the fiber damage threshold is exceeded.[13] This in turn limits the total energy that can be coupled into optical fibers for delivering the laser light to the imaged tissue. For deeply seated lesions in particular, the limited energy imposed by the fiber damage threshold could result in poor image quality and contrast. Beyrau et al.[14] indicated that the damage threshold for fused silica was 1 GW/cm^2. Robinson and Ilev[15] reported the peak power damage threshold of various commercial fibers at the laser wavelength of 532 nm and the pulse width of 10 ns. The measured damage threshold varied from 3.7 GW/cm^2 for a 100-μm-core-diameter fiber to 3.9 GW/cm^2 for a 200-μm-core-diameter fiber, and the corresponding pulse energy damage threshold varied from 2.9 to 9.7 mJ. They also reported that the damage threshold of their experimental 700-μm fiber was 0.86 GW/cm^2, which was similar to the 1 GW/cm^2 damage threshold level of the commercially available high-energy fiber from OFS Inc. (Fitel HCGMO200T 200 μm). For the *in vivo* clinical applications, including the intravascular and endoscopic photoacoustic imaging, the probe needs to be miniaturized, and the fiber diameters need to be in the range of a few hundred micrometers.[10,12] Also, in photoacoustic imaging, the laser pulse width is usually as low as 5 to 7 ns.[10,12,16] Assuming the laser pulse width is 6 ns and the fiber diameter is 400 μm, based on the 1 GW/cm^2 fiber damage threshold,[14,15] the maximum energy that can be coupled into the fiber is only about 7.5 mJ; if the fiber diameter is 200 μm, the maximum energy coupled is only about 1.9 mJ. Considering the coupling loss of optical fibers, the output energy would be even lower, which is far below the maximum permissible exposure (MPE)[17] and not enough for imaging deeper lesions. Therefore, increasing the fiber damage threshold is a critical issue for photoacoustic imaging applications.

The coreless fiber endcap can also reduce the optical damage at fiber end faces, and the anti-reflective (AR) coating can minimize the back-reflection. However, the fiber endcap and the AR coating can cause extra energy losses, including splicing loss. Moreover, the damage threshold is highly dependent on how the interface is prepared. Therefore the improvement on the fiber damage threshold is not predictable. In Ref. 15, a tapered-glass funnel was used to couple the laser light to a hollow glass waveguide. The maximum input energy was increased, but the total laser energy delivery efficiency was only 30%. Besides, the delivery system was complicated, and the coupling was a variable, and its cost was much higher

Address all correspondence to: Quing Zhu, University of Connecticut, Electrical and Computer Engineering Department, Storrs, CT 06269. Tel.: 860-486-5523; Fax: 860-486-2447; E-mail: zhu@engr.uconn.edu

0091-3286/2012/$25.00 © 2012 SPIE

than that for commercial silica fibers. Comparing with those methods, laser-pulse-stretching is a convenient and an effective technique to solve the fiber damage problem. It can reduce the peak power and increase the fiber damage threshold.[18] Ideally, the laser pulse can be stretched without losing optical energy. Pulse-stretching techniques include optical pulse stretching,[19–22] electronic pulse stretching,[23,24] pulse stretching by dispersion,[25–27] and pulse stretching using nonlinear materials.[28,29] In optical pulse stretching, optical components are used to split the incident laser pulse into two or more pulses, and an appropriate optical delay is introduced to each pulse. Recombination of all the delayed pulses then results in a stretched pulse. One typical example of an optical pulse stretching system is the ring cavity configuration using mirrors and beam-splitters. A square ring cavity was reported in an oscillator-amplifier copper vapor laser which stretched the laser pulse from 34 to 50 ns.[19] Multiple-ring-cavity configuration was reported to stretch the 8.4-ns laser pulse of Q-switched Nd:YAG laser to a 75-ns laser pulse with a peak power reduction to 10% and an efficiency of 83%.[20] An optical pulse stretcher composed of two optical cavities was reported to stretch a 24-ns laser pulse and also realized fast switching between different pulse durations (24, 60, 63, and 122 ns).[21] Among those methods of pulse stretching, the ring-cavity setup is easy and the cost is low.

In this paper, the effect of pulse stretching on photoacoustic imaging is studied by simulations and experiments. An initial 17-ns laser pulse measured at the half maximum (FWHM) was launched from a Ti:sapphire laser and stretched to 27 and 37 ns by a ring-cavity nanosecond laser pulse stretching system in order to increase the fiber damage threshold. The peak of the 37-ns stretched pulse reduced to 42% of the original pulse and the stretched pulse increased the fiber damage threshold by 1.5-fold, which is significant in delivering higher total energy for deep-tissue imaging. Photoacoustic signals from different target sizes obtained with different pulse durations were simulated. Three ultrasound transducers centered at 1.3-, 3.5-, and 6-MHz frequencies of 120, 80, and 80% fractional bandwidth were used. The simulations were validated by experimental results using a broadband hydrophone with a flat frequency response from 1 to 10 MHz. In addition, quantitative comparisons of photoacoustic images obtained with three ultrasound transducers of the same center frequency and bandwidth as the simulation showed that the image quality was not affected by stretching the pulse using the reported ring-cavity technique. To the best of our knowledge, this is the first study applying laser-pulse stretching to photoacoustic imaging applications. The simulations and experimental results can be used as a reference for laser-pulse stretcher designs on compromising total energy delivery to tissue and fiber damage threshold.

2 Methods

2.1 *Simulation Method*

The MATLAB k-Wave toolbox[30] was used to simulate the time-domain photoacoustic signal, and the fast Fourier transform (FFT) was applied to obtain the frequency domain spectrum. The *k*-Wave simulation functions are based on a *k*-space pseudo-spectral time domain solution to couple first-order acoustic equations for homogenous and heterogeneous media. In our *k*-Wave simulations, a Gaussian pulse beam was uniformly applied to a disc target, and a single-element sensor was used to detect the acoustic wave within a two-dimensional homogeneous medium. To simulate the effects of the limited bandpass of the transducers, different Gaussian bandpass filters were applied to the frequency domain of the simulated time-domain photoacoustic signals. Three different ultrasound transducers of center frequencies of 1.3, 3.5, and 6 MHz with fractional bandwidths of 120, 80, and 80%, respectively, were used in the simulations. Transducers in the central frequency range of 3 to 10 MHz are typically used in clinical ultrasound systems. Transducers in the lower frequency range of 1 to 2 MHz are often used by the research community for photoacoustic imaging applications.

2.2 *Ring-Cavity Pulse Stretching System*

One way to achieve the objective of reducing the laser peak intensity with only a minimal energy loss is to use the pulse stretcher realized by an optical triangular ring cavity.[20] As shown in Fig. 1, an initial input laser pulse $I_0(t)$ is partially reflected by a fractional amount of R_{BS} and partially transmitted by (1-R_{BS}) through the beam-splitter, where R_{BS} is the reflectivity of the beam-splitter. This transmitted pulse circulates inside the ring cavity and is then reflected and transmitted again and again by the beam-splitter. The successive laser pulses from the ring cavity have optical delay times of $\tau, 2\tau, \ldots k\tau$, where k is an integer that represents the number of round trips in the ring cavity. As a result, the initial input laser pulse is divided into many pulses with different optical delay times, so the output laser pulse $I(t)$ is given by the superposition of each smaller amplitude pulses to achieve the pulse stretching. This is shown by the equation:

$$\begin{aligned} I(t) &= R_{BS}I_0(t) + (1-R_{BS})^2 I_0(t-\tau) \\ &\quad + (1-R_{BS})^2 R_{BS} I_0(t-2\tau) + \cdots \\ &= R_{BS}I_0(t) + (1-R_{BS})^2 \sum_{k=1}^{K} R_{BS}^{k-1} I_0(t-k\tau). \end{aligned} \tag{1}$$

For pulsed lasers in the range of micro-second to nanosecond, the energy density varies as a function of the square root of the pulse duration, and the laser damage threshold is given by Eq. (2):[31,32]

$$\mathrm{LDT}(Y) = \mathrm{LDT}(X)\sqrt{\frac{Y}{X}}, \tag{2}$$

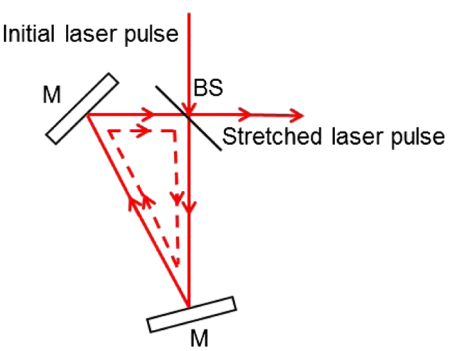

Fig. 1 Schematic of laser-pulse stretching system based on a triangular ring cavity. M: mirror, BS: beam-splitter.

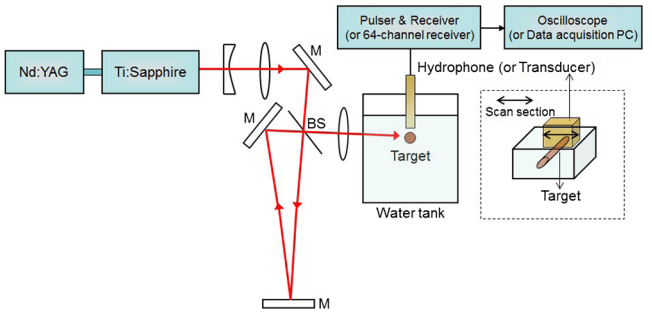

Fig. 2 Experimental setup of photoacoustic imaging using stretched laser pulse. M: mirror, BS: beam-splitter.

where LDT is the laser damage threshold, X is original pulse duration, and Y is the new pulse duration. Therefore, the fiber input end damage threshold is proportional to the square root of the laser pulse width.

2.3 *Experimental Setup*

The photoacoustic tomography (PAT) experimental setup is shown in Fig. 2. A Ti:sapphire laser (Symphotics TII, LS-2134) pumped with a Q-switched Nd:YAG laser (Symphotics TII, LS-2122) operated at a wavelength of 745 nm with a FWHM of 17 ns and a repetition rate of 15 Hz. The laser beam was expanded with a Galilean telescope and then reflected into the cavity of the triangular ring pulse stretcher. The beam-splitter had a reflectivity/transmission ratio of 40/60, and the ring cavity length was 4.5 m. The energy throughput of the pulse stretcher was 92%. Most of the 8% energy loss resulted from the divergence of the laser beam, which expanded the beam size beyond that of the mirrors and beam-splitter. The use of larger-size optical components will significantly decrease the loss. A 0.5-mm-diameter music wire, and tube of inner diameter 0.58 mm and outer diameter 0.97 mm filled with rat blood were used as targets to generate photoacoustic waves. Two sets of experiments were performed to compare photoacoustic measurement data and image quality obtained with the original and stretched laser pulses. In the photoacoustic measurement experiment, a broadband hydrophone (Force Institute, Copenhagen) with a flat frequency response from 1 to 10 MHz was used. Its output was amplified by a Panametrics receiver (Panametrics 5072PR) and sampled by a digital oscilloscope of 300-MHz bandwidth (Tektronix, TDS3032). The corresponding bandpass filters were applied in software to simulate the transducers. In the photoacoustic imaging experiment, three ultrasound transducers centered at 1.3 MHz (Vermon, France), 3.5 MHz (GE, Medical Systems), 6 MHz (W.L. Gore & Associates Inc.) of 120, 80, and 80% fractional bandwidth were used, respectively. Both the wire and tube were imaged in the transverse directions. The receiving electronics consisted of 64 parallel preamplifiers of 20-dB gain and outputs of the preamplifiers were multiplexed to two parallel channels for further amplification, low pass filtering and analog-to-digital (A/D) conversion. The system was controlled with a custom C-language software on the host computer through the two digital I/O cards connected to the A/D. Delay and sum beam-forming algorithm was used for photoacoustic image reconstruction.

2.4 *Imaging Quality Comparison*

To quantitatively compare the image quality using the original and stretched pulses, the image contrast and resolution were calculated from the target response. The beam line across the center of the target was extracted. The ratio of peak value and the averaged background value was used to estimate the contrast, and FWHM was used to estimate the temporal resolution.

3 Simulation and Experimental Results

3.1 *Simulations*

The photoacoustic spectrum is affected by using laser pulses of different widths and targets of different sizes. Figure 3 shows the FFT of photoacoustic signals obtained with FWHM of 6- and 50-ns laser pulses of both the same energy. Figure 3(a) and 3(b) shows the results of using 0.25- and 2-mm-diameter targets, respectively. For the 0.25-mm-diameter target, the spectrum shifted to a lower frequency range, and a small fraction of the amplitudes of both the lower and higher frequency components was lost as the pulse width increased. For the 2-mm-diameter target, the amplitudes of the lower frequency components were almost the same, but that of the higher-frequency components decreased a little as the pulse width increased. In general, the photoacoustic signal generated by the 6-ns laser pulse was higher than that generated by 50-ns laser pulse, which was due to the more efficient acoustic

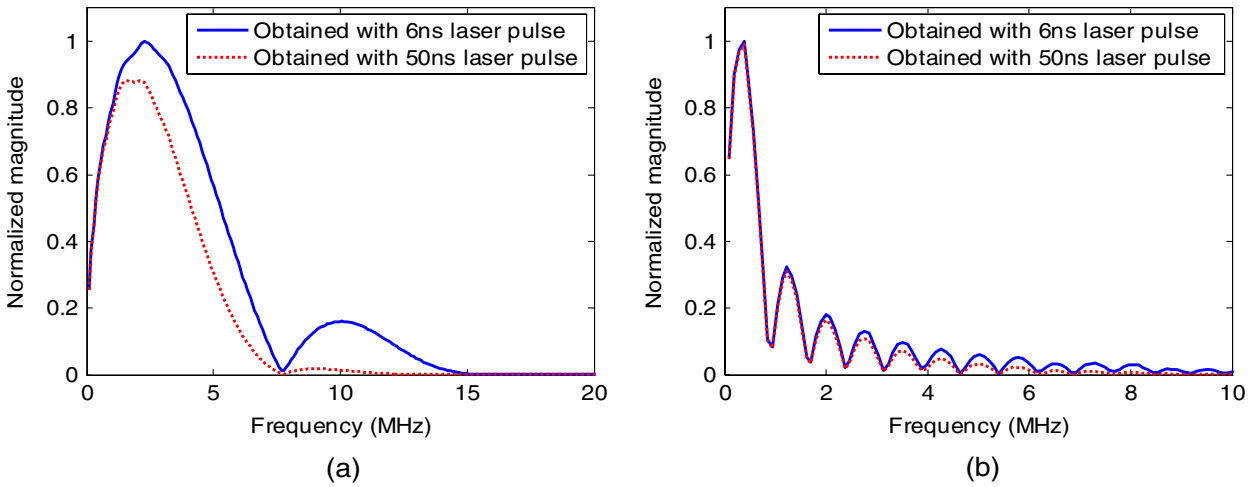

Fig. 3 Frequency-domain photoacoustic signals obtained with 6- and 50-ns laser pulses. (a) 0.25-mm-diameter target, (b) 2-mm-diameter target.

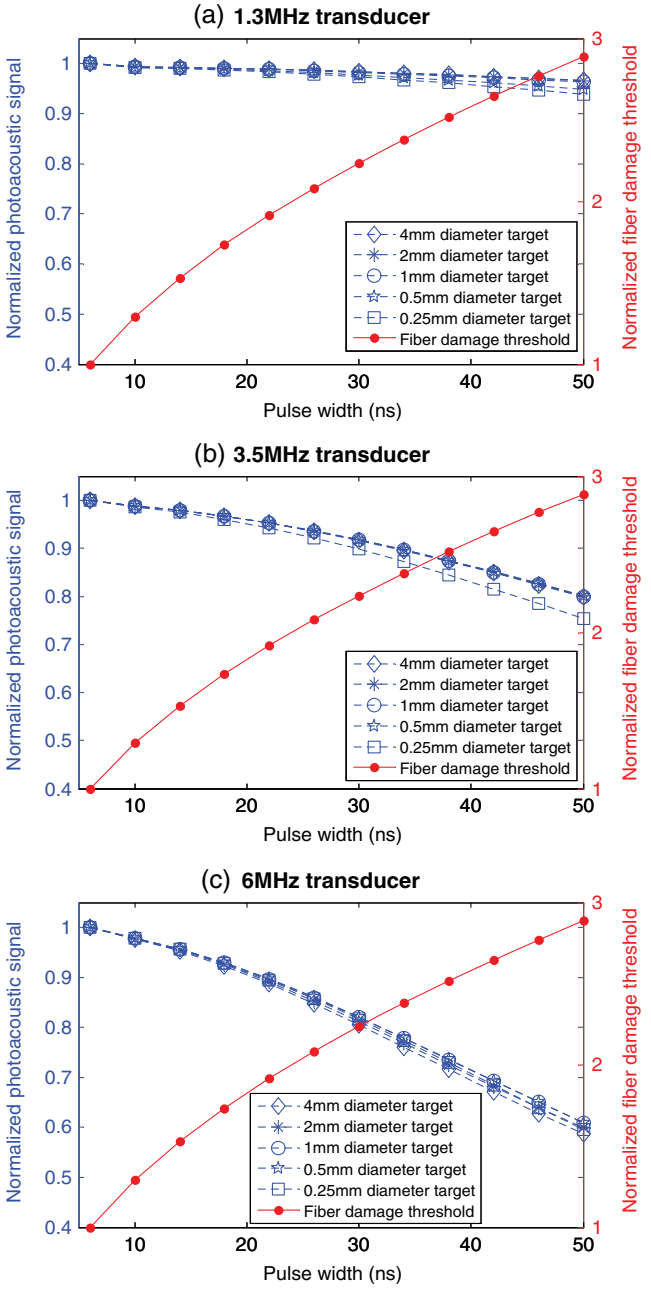

Fig. 4 Simulations of normalized photoacoustic signal and normalized fiber damage threshold versus laser pulse width. The photoacoustic signal was obtained with (a) 1.3-MHz transducer, (b) 3.5-MHz transducer, (c) 6-MHz transducer.

wave generation achieved by shorter pulses.[33] In addition, by comparing Fig. 3(a) and 3(b), the main peak of the spectrum shifted to a lower frequency as the target size was increased.

To systematically study the pulse width effect, photoacoustic signals obtained with equal-energy pulse widths ranging from 6 to 50 ns were simulated using MATLAB k-Wave toolbox. In the simulations, different target sizes with diameters of 4, 2, 1, 0.5, and 0.25 mm were used to generate photoacoustic signals. The photoacoustic signal was simulated by integrating the frequency domain signals that can be received by each ultrasound transducer. The results using the three transducers are shown in Fig. 4(a), 4(b), and 4(c), respectively. The left y-axis of each figure represents the photoacoustic signals, which are normalized to the photoacoustic signal obtained with the 6-ns laser pulse. The right *y*-axis represents the fiber damage threshold, which is normalized to the fiber damage threshold by using 6-ns laser pulse. If other conditions are fixed, the fiber damage threshold is proportional to the square root of the laser-pulse width based on Eq. (2). The simulation results for the photoacoustic signals are shown in dotted lines, and that of the fiber damage threshold are shown in solid lines. For all the three transducers, the photoacoustic signals decreased as the pulse width increased; at the same time, the fiber damage threshold increased. Compared with the 6-ns pulse, the photoacoustic signals obtained with the 50-ns pulse was more than 94, 75, and 58% for the 1.3-, 3.5-, and 6-MHz transducers, respectively. Following this, the fiber damage threshold increased by 2.9-fold. In some cases, the laser pulse might not need to be stretched that much as from 6 to 50 ns, so that the photoacoustic signal was almost not affected. For example, if stretching the laser pulse from 6 to 14 ns, the photoacoustic signal of 0.5-mm-diameter target obtained by 1.3-, 3.5-, 6-MHz transducer was about 99.1, 97.9, and 95.7, respectively, after stretching the pulse, and, as a reward, the fiber damage threshold was increased by 1.5-fold. These results are useful for designing a laser pulse stretcher in order to increase the fiber damage threshold to ensure that higher laser energy can be delivered to the imaged tissue by fibers. Figure 4 also shows that the photoacoustic signals were less sensitive to target size for the three types of transducers and the range of target sizes evaluated.

3.2 *Experimental Results*

The triangular ring-cavity laser-pulse stretching system stretched the initial 17-ns (FWHM) laser pulse to 27- and 37-ns laser pulses as shown in Fig. 5. The peak intensity of the 27- and 37-ns laser pulse was reduced to about 58 and 42% of the initial 17-ns pulse, and the fiber damage threshold was increased by 1.3- and 1.5-fold, respectively.

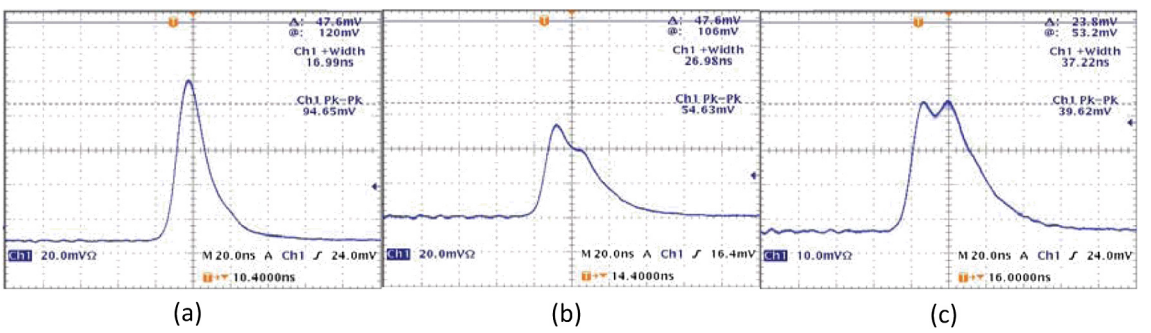

Fig. 5 Profile of laser pulses: (a) initial 17-ns laser pulse; (b) stretched 27-ns laser pulse; (c) stretched 37-ns laser pulse.

3.2.1 *Experimental validations*

The simulations were validated using a hydrophone. The photoacoustic signals of the 0.5-mm-diameter music wire obtained with pulse widths of 17, 27, and 37 ns all having the same energy, and the aforementioned transducers are shown in Fig. 6. The corresponding bandpass filters were applied to the photoacoustic signals received by hydrophone and averaged over four experimental data. The left *y*-axis of each figure corresponds with the normalized photoacoustic signals, and the right *y*-axis corresponds with the normalized fiber damage threshold. Both simulation and experimental results of photoacoustic signals are shown in dotted lines, and that fiber damage threshold is shown in solid line. The experimental results show

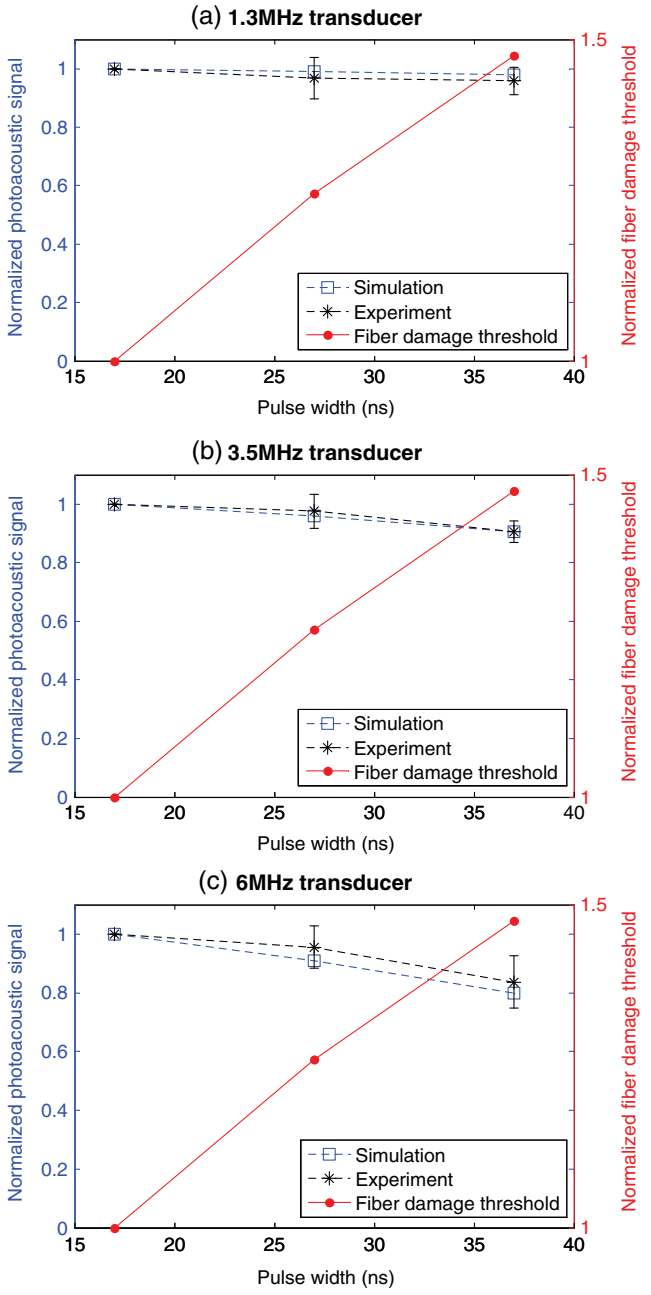

Fig. 6 Simulations and experimental results of normalized photoacoustic signal and normalized fiber damage threshold versus laser-pulse width. The photoacoustic signal was obtained with (a) 1.3-MHz transducer; (b) 3.5-MHz transducer; (c) 6-MHz transducer.

that using the 1.3-MHz transducer, the photoacoustic signals obtained with the 27- and 37-ns stretched pulse are about 96.7% (std 7.0%) and 95.8% (std 4.7%), respectively, of the initial 17-ns laser pulse and agree well with the simulation results of 99.2 and 97.9%. Again for the 3.5-MHz transducer, the photoacoustic signals obtained with those stretched pulses are about 97.6% (std 5.8%) and 90.6% (std 3.5%) of the initial 17-ns laser pulse; this also agrees well with the simulation results of 96.0 and 90.7%. Finally, for the 6-MHz transducer, the photoacoustic signals obtained with the stretched pulses are about 95.5% (std 7.2%) and 83.7% (std 8.8%) of the initial 17-ns laser pulse; this agrees well with the simulation results of 90.8 and 79.5%. At the same time, by stretching the laser pulse to 27 and 37 ns, the fiber damage threshold was increased by 1.3- and 1.5-fold, which is significant in delivering higher-energy laser light to image deeply seated targets. Both simulation and experimental results indicate that, by stretching the laser pulse from 17 to 37 ns, the fiber damage threshold is improved without much loss of photoacoustic signal.

3.2.2 *Imaging comparisons*

The photoacoustic images of 0.5-mm-diameter music wire obtained with pulse widths of 17 and 37 ns having the same energy, and the aforementioned transducers are shown in

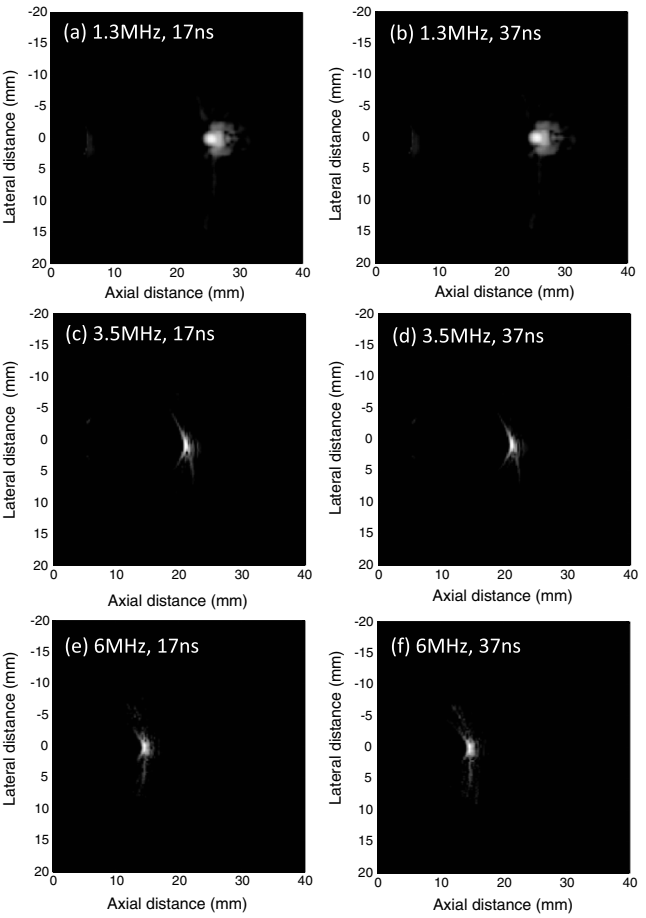

Fig. 7 Photoacoustic images of 0.5-mm-diameter music wire obtained with (a) 1.3-MHz transducer, 17-ns laser pulse; (b) 1.3-MHz transducer, same energy of stretched 37-ns laser pulse; (c) 3.5-MHz transducer, 17-ns laser pulse; (d) 3.5-MHz transducer, same energy of stretched 37-ns laser pulse; (e) 6-MHz transducer, 17-ns laser pulse; (f) 6-MHz transducer, same energy of stretched 37-ns laser pulse.

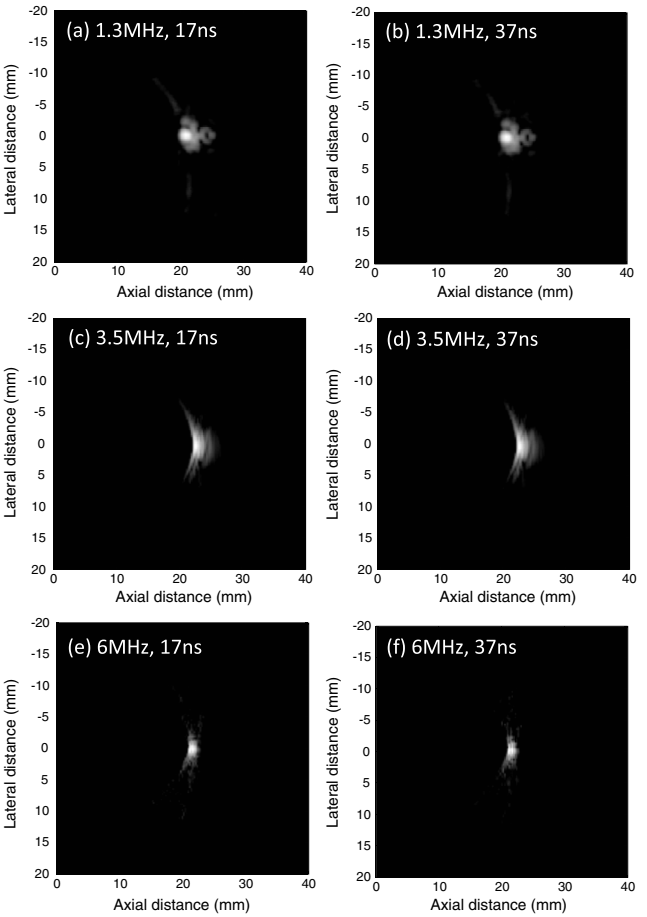

Fig. 8 Photoacoustic images of blood tube obtained with (a) 1.3-MHz transducer, 17-ns laser pulse; (b) 1.3-MHz transducer, same energy of stretched 37-ns laser pulse; (c) 3.5-MHz transducer, 17-ns laser pulse; (d) 3.5-MHz transducer, same energy of stretched 37-ns laser pulse; (e) 6-MHz transducer, 17-ns laser pulse; (f) 6-MHz transducer, same energy of stretched 37-ns laser pulse.

Fig. 7(a) and 7(b), 7(c) and 7(d), 7(e) and 7(f), respectively, in log-scale. The dynamic range of the image was set to 30 dB. The scan section of the transducer was placed perpendicular to the target during imaging. The image quality was not affected by stretching the pulse by visually comparing those images.

The photoacoustic images of blood tube obtained with pulse widths of 17 and 37 ns have the same energy, and the aforementioned transducers are shown in Fig. 8(a) and 8(b), 8(c) and 8(d), 8(e) and 8(f), respectively, in log-scale. Similar as the images of music wire, the image quality of the blood tube was not affected by stretching the pulse by visually comparing those images. Note that the images of Figs. 7(c) and 7(d) and 8(c) and 8(d) were slightly defocused. This 3.5-MHz transducer was designed for cardiac imaging and had the acoustic lens of 7-cm-elevation focal depth. However, the targets were located around 2 cm for comparison with the images obtained by 1.3 and 6 MHz linear arrays with the elevation focal depth fixed at 2 cm.

The image contrast and resolution were calculated to compare the image quality quantitatively. Figure 9 illustrates the contrast and resolution calculation. Figure 9(a) shows the beam line across the center of the target image. The signal in the dash rectangular area was the background, and the contrast was estimated by calculating the ratio of the peak value and the averaged background value. Figure 9(b) is the zoomed-in portion of solid rectangular area in Fig. 9(a). The FWHM was calculated to estimate the temporal resolution. The quantitative comparison results are shown in Table 1. Three averages were done for each ratio. For both music wire and blood tube targets, the contrast and the resolution did not show much difference between 17- and 37-ns laser pulses.

By stretching the laser pulse from 17 to 37 ns, the fiber damage threshold increased by 1.5-fold. Therefore, the upper-limit energy that can be delivered by the fiber also increased by 1.5-fold. If MPE is not exceeded, higher energy can be coupled into the fiber so that higher energy can be delivered to the imaged tissue by stretching the laser pulse. Figure 10 shows the comparisons of music wire images using 17-ns pulse and 1.5-fold energy of stretched 37-ns pulse. Similar to the quantitative comparison in Table 1, Table 2 shows the contrast and resolution ratio of 1.5-fold energy of stretched 37-ns pulse and initial 17-ns pulse. In this case, the image contrast is improved after stretching the pulse.

4 Discussion and Summary

A series of simulations and experiments have been completed to investigate the laser-pulse stretching effect on photoacoustic

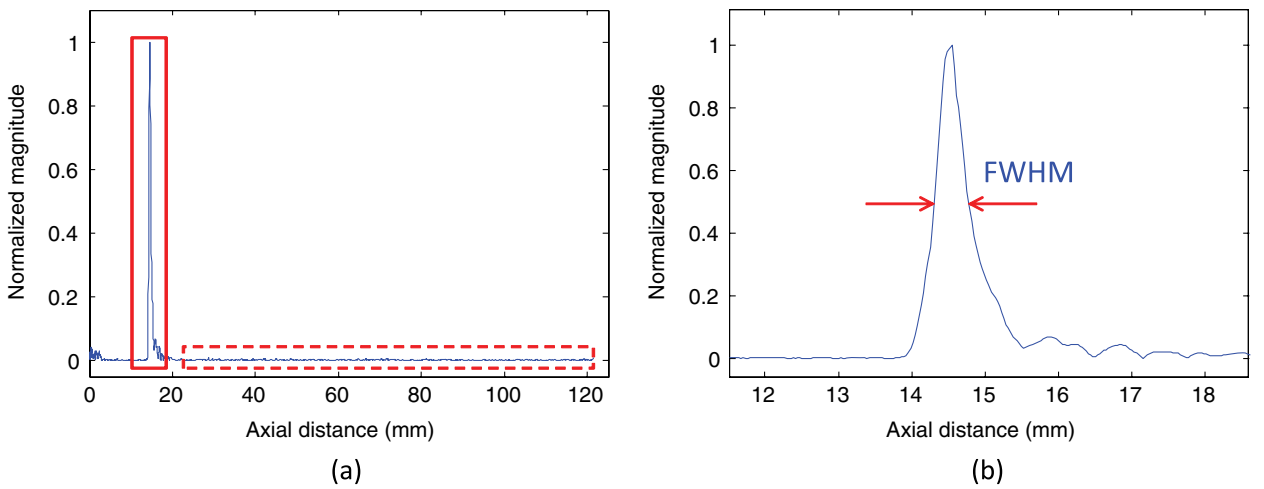

Fig. 9 The beam line across the center of the target: (a) illustration of contrast calculation; (b) zoomed-in of solid rectangular area in Fig. 9(a) to illustrate resolution calculation.

Table 1 Photoacoustic image quality comparison using same energy of 17- and 37-ns pulses. Contrast (resolution) ratio = Contrast (resolution) obtained with 37-ns laser pulse/17-ns laser pulse. (a) Music wire comparison. (b) Blood tube comparison.

	Contrast ratio (Std)	Resolution ratio (Std)
(a)		
1.3-MHz transducer	0.976 (0.010)	0.987 (0.011)
3.5-MHz transducer	0.929 (0.035)	1.076 (0.069)
6-MHz transducer	0.892 (0.007)	0.979 (0.036)
(b)		
1.3-MHz transducer	0.991 (0.005)	0.993 (0.012)
3.5-MHz transducer	0.932 (0.025)	0.991 (0.032)
6-MHz transducer	0.892 (0.026)	1.012 (0.020)

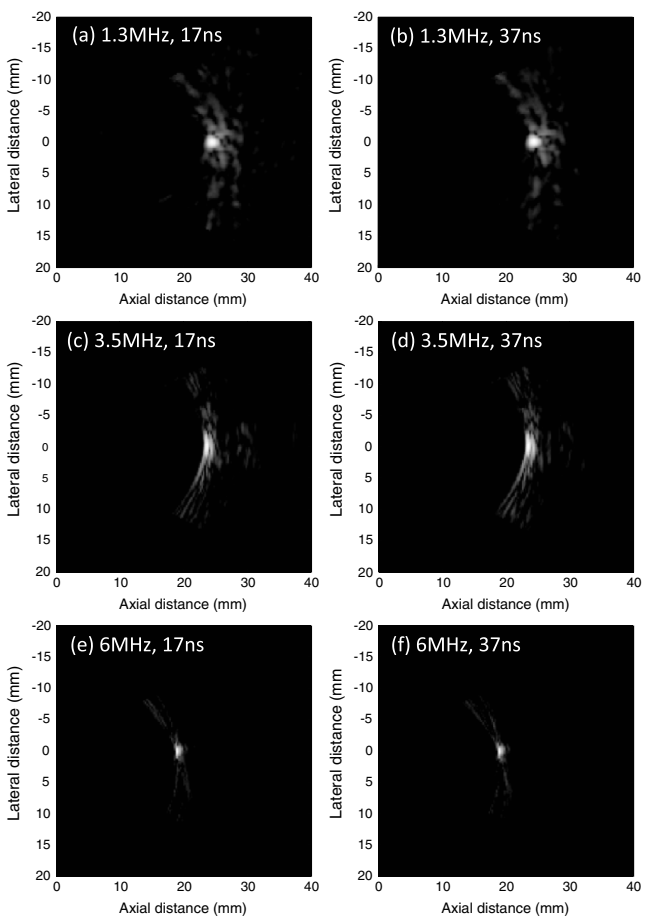

Fig. 10 Photoacoustic images of 0.5-mm-diameter music wire obtained with (a) 1.3-MHz transducer, 17-ns laser pulse; (b) 1.3-MHz transducer, 1.5-fold energy of stretched 37-ns laser pulse; (c) 3.5-MHz transducer, 17-ns laser pulse; (d) 3.5-MHz transducer, 1.5-fold energy of stretched 37-ns laser pulse; (e) 6-MHz transducer, 17-ns laser pulse; (f) 6-MHz transducer, 1.5-fold energy of stretched 37-ns laser pulse.

Table 2 Photoacoustic image quality comparison using 17-ns and 1.5-fold energy of 37-ns pulses.

	Contrast ratio (Std)	Resolution ratio (Std)
1.3-MHz transducer	1.477 (0.067)	1.000 (0.020)
3.5-MHz transducer	1.334 (0.033)	1.020 (0.057)
6-MHz transducer	1.264 (0.030)	0.976 (0.041)

imaging. The results presented for the laser-pulse width range and target size range show that by stretching the laser pulse, the image quality is not affected and the fiber damage threshold is increased. This helps protect the fiber input face during high-energy photoacoustic imaging of deeply seated tissue. Provided the MPE is not exceeded, higher energy can be coupled into the fiber for delivery to the imaged tissue to improve the signal-to-noise ratio. In addition, some of the 8% energy loss during pulse stretching resulted from the divergence of the laser beam, which was not fit for our current mirror and beam-splitter size. If we use larger size mirrors and beam-splitter, this triangular ring-cavity laser-pulse stretcher would have higher-energy efficiency, and the only energy loss could come from the slight loss of mirrors and beam-splitter. One other problem of the ring-cavity pulse-stretching system right now is that it is bulky for clinical use as the cavity length used for the pulse stretching was 4.5 m. To solve this problem, we plan to use a laser-pulse stretcher made from fibers.[34] The laser beam was split into many parts and then input into fibers with different lengths to induce optical delays, and the output laser light with different optical delays recombined together to generate a longer pulse with the same total energy.

The simulation and measurement reported in this paper have focused on the 6- to 50-ns pulse width range and the 0.25- to 4-mm target diameter range, which is about one to two times ultrasound wavelength for typical 1- to 8-MHz transducers. In this range of target size, the stress confinement condition is stringently satisfied. The pulse-stretching effect on the detected photoacoustic signals is less sensitive to target properties, including the size, the absorption, and scattering properties. However, if the optical penetration depth in the target or the fully penetrated target size is smaller than the range studied, the PA signals will be affected more by stretching the laser pulse. The detected photoacoustic signals depend on the target sizes or optical penetration depth (whichever is smaller) and ultrasound transducer central frequencies.

In summary, we report a laser-pulse stretching scheme for efficiently delivering laser energy to tissue while reducing the peak intensity for minimizing the fiber damage. To demonstrate the principle, we have compared photoacoustic signals and images obtained with 17 ns, and the stretched 27- and 37-ns laser pulses. The peak power of the stretched 37-ns pulse was reduced to 42% of the original pulse to significantly reduce the damage of the input fiber. Simulations and experimental results showed that the stretching technique increased the fiber damage threshold, and the image quality was not affected.

Acknowledgments

This research was supported by NIH R01CA151570.

References

1. M. Xu and L. V. Wang, "Photoacoustic imaging in biomedicine," *Rev. Sci. Instrum.* **77**(4), 041101 (2006).
2. L. V. Wang, "Prospects of photoacoustic tomography," *Med. Phys.* **35**(12), 5758–5767 (2008).
3. J. Oh et al., "Three-dimensional imaging of skin melanoma in vivo by dual-wavelength photoacoustic microscopy," *J. Biomed. Optic.* **11**(3), 34032 (2006).
4. J. Gamelin et al., "A real-time photoacoustic tomography system for small animals," *Opt. Express* **17**(13), 10489–10498 (2009).
5. J. Gamelin et al., "Curved array photoacoustic tomographic system for small animal imaging," *J. Biomed. Optic.* **13**(2), 024007 (2008).
6. X. Wang et al., "Noninvasive laser-induced photoacoustic tomography for structural and functional in vivo imaging of the brain," *Nat. Biotechnol.* **21**(7), 803–806 (2003).
7. S. Manohar et al., "The Twente Photoacoustic Mammoscope: system overview and performance," *Phys. Med. Biol.* **50**(11), 2543–2557 (2005).
8. A. Aguirre et al., "Co-registered three-dimensional ultrasound and photoacoustic imaging system for ovarian tissue characterization," *J. Biomed. Opt.* **14**(5), 054014 (2009).
9. A. Aguirre et al., "Potential role of co-registered photoacoustic and ultrasound imaging in ovarian cancer detection and characterization," *Transl. Oncol.* **4**(1), 29–37 (2011).
10. B. Wang et al., "Intravascular photoacoustic imaging," *IEEE J. Quant. Electron.* **16**(3), 588–599 (2010).
11. B. Wang et al., "Detection of lipid in atherosclerotic vessels using ultrasound-guided spectroscopic intravascular photoacoustic imaging," *Opt. Express* **18**(5), 4889–4897 (2010).
12. J. Yang et al., "Photoacoustic endoscopy," *Opt. Lett.* **34**(10), 1591–1593 (2009).
13. S. Seidel and G. Phillipps, "Pulse lengthening by intracavity stimulated Brillouin scattering in a Q-switched, phase-conjugated Nd:YAG laser oscillator," *Appl. Opt.* **32**(36), 7408–7417 (1993).
14. F. Beyrau et al., "Application of an optical pulse stretcher to coherent anti-Stokes Raman spectroscopy," *Opt. Lett.* **29**(20), 2381–2383 (2004).
15. R. A. Robinson and I. K. Ilev, "Design and optimization of a flexible high-peak-power laser-to-fiber coupled illumination system used in digital particle image velocimetry," *Rev. Sci. Instrum.* **75**(11), 4856–4862 (2004).
16. R. E. Kumon, C. X. Deng, and X. Wang, "Frequency-domain analysis of photoacoustic imaging data from prostate adenocarcinoma tumors in a murine model," *Ultrasound Med. Biol.* **37**(5), 834–839 (2011).
17. Laser Institute of America, "American National Standard for Safe Use of Lasers ANSI Z136. 1-2000," (American National Standards Institute, Inc., 2000).
18. S. Pflüger et al., "Fiber-optic transmission of stretched pulses from a Q-switched ruby laser," *Appl. Opt.* **35**(25), 5165–5169 (1996).
19. M. Amit et al., "Temporal and spatial properties of an oscillator-amplifier copper vapor laser," *Opt. Commun.* **62**(2), 110–114 (1987).
20. J. Kojima and Q. Nguyen, "Laser pulse-stretching with multiple optical ring cavities," *Appl. Opt.* **41**(30), 6360–6370 (2002).
21. A. Burkert et al., "Pulse stretcher with variable pulse length for excimer laser applications," *Rev. Sci. Instrum.* **81**(3), 033014 (2010).
22. R. Khare et al., "A novel confocal optical pulse stretcher for laser pulses," *Opt. Commun.* **282**(19), 3850–3853 (2009).
23. R. V. Lovberg, E. R. Wooding, and M. L. Yeoman, "Pulse stretching and shape control by compound feedback in a Q-switched ruby laser," *IEEE J. Quant. Electron.* **11**(1), 17–21 (1975).
24. L. Verluyten et al., "Laser pulse stretching via enhanced closed loop control with slow Q-switching," *Nucl. Instrum. Meth. Phys. Res. A* **292**(2), 313–318 (1990).
25. P. Maine et al., "Generation of ultrahigh peak power pulses by chirped pulse amplification," *IEEE J. Quant. Electron.* **24**(2), 398–403 (1988).
26. J. Azuma et al., "Optical detection system using time structure of UVSOR for combined laser-SR experiments," *Nucl. Instrum. Meth. Phys. Res. A* **467–468**(Part 2), 1455–1457 (2001).
27. A. K. Sharma et al., "Characteristics of a stable, injection Q-switched Nd:phosphate glass regenerative amplifier for a chirped pulse amplification based Table Top Terawatt laser system," *Opt. Commun.* **252**(4–6), 369–380 (2005).
28. G. Bergamasco et al., "Passive pulse stretching in an Nd:glass laser," *Opt. Quant. Electron.* **25**(4), 271–273 (1993).
29. P. Dekker, J. M. Dawes, and J. A. Piper, "2.27-W Q-switched self-doubling Yb:YAB laser with controllable pulse length," *J. Opt. Soc. Am. B* **22**(2), 378–384 (2005).
30. B. E. Treeby and B. T. Cox, "k-Wave: Matlab toolbox for the simulation and reconstruction of photoacoustic wave fields," *J. Biomed. Optic.* **15**(2), 021314 (2010).
31. J. Bisson et al., "Laser damage threshold of ceramic YAG," *Jpn. J. Appl. Phys.* **42**(Part 2, No. 8B), 1025–1027 (2003).
32. H. Kessler, "Laser damage thresholds of optical coatings, UV-NIR," Technical Reference, CVI Technical Optics Document #20041108.
33. T. J. Allen, B. T. Cox, and P. C. Beard, "Generating photoacoustic signals using high-peak power pulsed laser diodes," *Proc. SPIE* **5696**, 233–242 (2005).
34. D. Hanna and J. W. Mitchell, "A laser pulse stretcher made from optical fibres," *Nucl. Instrum. Meth. Phys. Res. A* **324**(1–2), 14–18 (1993).